Available online at www.sciencedirect.com
ScienceDirect
Journal of Solid State Chemistry 180 (2007) 2775–2784
JOURNAL OF SOLID STATE CHEMISTRY
www.elsevier.com/locate/jssc

Lamellar structures in neodymium borides

L. Kienle[a,*], V. Babizhetskyy[a], V. Duppel[a], R. Guérin[b], A. Simon[a]

[a]Max-Planck-Institut für Festkörperforschung, Heisenbergstr. 1, 70569 Stuttgart, Germany
[b]Laboratoire de Chimie du Solide et Inorganique Moléculaire, UMR CNRS 6511, Université de Rennes 1, Institut de Chimie, Campus de Beaulieu, Avenue du Général Leclerc, F-35042 Rennes Cedex, France

Received 20 June 2007; received in revised form 30 July 2007; accepted 6 August 2007
Available online 23 August 2007

Abstract

Samples with the nominal composition Nd_2B_5 contain strongly disordered crystals composed of nanosized (100) lamellae. Most commonly, a polysynthetic twinning based on a fourfold rotation separates the lamellae at coherent boundaries. The structure of the twin interface contains a pseudo fourfold arrangement of B atoms as derived from electron microscopy techniques. Such pseudo-symmetry serves for a rationalization of the twinning. Additionally, a chemical intergrowth of Nd_2B_5 and NdB_4 lamellae based on related structural building units can be observed. Further HRTEM examinations allow the identification of a new structural variant of neodymium borides.

Keywords: Electron microscopy; Disordered structure; X-ray diffraction; Rare earth metal compounds; Borides; Intergrowth phases; Twinning

1. Introduction

Lamellar structures have been recognized as a focal point of solid-state sciences due to their broad spectrum of physical properties and fascinating chemical aspects. Among them, 1D disordered intergrowth phases with a variable thickness of consecutive lamellae are most common. Homogeneous crystals of this type can be characterized by the interconnection of adjacent lamellae, e.g. as polysynthetic twins. The special case of a "phasoid" [1] is met for inhomogeneous crystals composed of chemically different lamellae. The structure determination of intergrowth phases bears many challenges due to space averaging of lamellae smaller than the X-ray coherence length. Hence, the standard methods are likely to fail, and only a combined methodical approach with the focus on electron microscopy techniques allows the full characterization of all lamellar components and their interconnection [2,3]. Phasoids and polysynthetic twins of rare earth metal (*Ln*) compounds have been reported in many instances, e.g. for boride carbides [4]; however, lamellar intergrowth phases of binary borides have not yet been reported.

The Nd–B phase diagram [5,6] contains four phases, namely NdB_{66}, NdB_6, NdB_4 (ThB_4-type, $P4/mbm$, [7–9] and Nd_2B_5. The known crystal structures of Ln_2B_5 belong to the simple Sm_2B_5-type (also for $Ln = Gd$, $P2_1/c$, [10,11]) and the more complex Pr_2B_5-type structure ($C2/c$, [12]), respectively. According to a recent analysis [9], the structure of Nd_2B_5 was assigned to the Pr_2B_5-type structure, however, accurate X-ray studies on large single crystals indicated deviations. The diffraction patterns showed very weak reflections in addition to those expected for the Pr_2B_5-type, and first attempts of indexing indicated a threefold superstructure along a^*. The number and intensity of the superstructure reflections inhibited a structure solution. Furthermore, X-ray analyses of very small crystals and powders gave no indications of any superstructure. This inconsistency called for the presence of large domains in large crystals. These domains produce the superstructure as an artifact of superposition. Further information concerning the structure was not available by metallographic and X-ray investigations, hence, electron microscopy techniques were selected for the analysis of the domains.

*Corresponding author. Fax: +49 07116891091.
E-mail address: L.Kienle@fkf.mpg.de (L. Kienle).

0022-4596/$ - see front matter © 2007 Elsevier Inc. All rights reserved.
doi:10.1016/j.jssc.2007.08.001

2. Results

2.1. X-ray analyses and basic tem observations

The X-ray diffraction patterns of apparently large crystals can be rationalized in terms of twinning of Pr_2B_5-type domains with accurately defined relative orientations. At first glance, the superposition pattern of Fig. 1a contains the layers $hk0_1$ (zone axis [001]) and $h0l_2$ (zone axis [010]) for the twin components 1 and 2, and the twinning produces characteristic coincidences of the reflections $hk0_1$ ($k = 6n$) and $h0l_2$ ($l = 6n$), cf. to the grids in Fig. 1a. Hence, reticular pseudo-merohedry is present with a fourfold rotation axis along [100]* acting as the twin element. This finding also expects the presence of domains in [0−10] (component 3) and [00−1] orientations; however, due to the overlap of $\langle 001 \rangle$ patterns only contributions from 3 could be identified in the diffraction pattern of Fig. 1a. Actually, only a small amount of sufficiently large domains of 3 is present as indicated by the faint intensity of $20{-}2_3$ (see arrow) versus $20{-}2_2$ (see asterisk), cf. inset of Fig. 1a.

The three-dimensional arrangement of the domains can be calculated by applying the following relations for direct (P-matrix) and reciprocal space (Q-matrix), respectively:

$$\begin{pmatrix} a' \\ b' \\ c' \end{pmatrix} = P \begin{pmatrix} a \\ b \\ c \end{pmatrix} \text{ and } \begin{pmatrix} x' \\ y' \\ z' \end{pmatrix} = Q \begin{pmatrix} x \\ y \\ z \end{pmatrix}$$

$$\text{with } P = \begin{pmatrix} 3 & 0 & 2 \\ 0 & 0 & 1 \\ 0 & \overline{1} & 0 \end{pmatrix} \text{ and } Q = \begin{pmatrix} 1/3 & 0 & 0 \\ \overline{2/3} & 0 & 1 \\ 0 & \overline{1} & 0 \end{pmatrix}.$$

This transformation simulates a nearly rectangular supercell which is three times larger with respect to the untwinned Nd_2B_5 (cf. [9], $a' = 42.752(2)$ Å, $b' = 7.2522(3)$ Å,

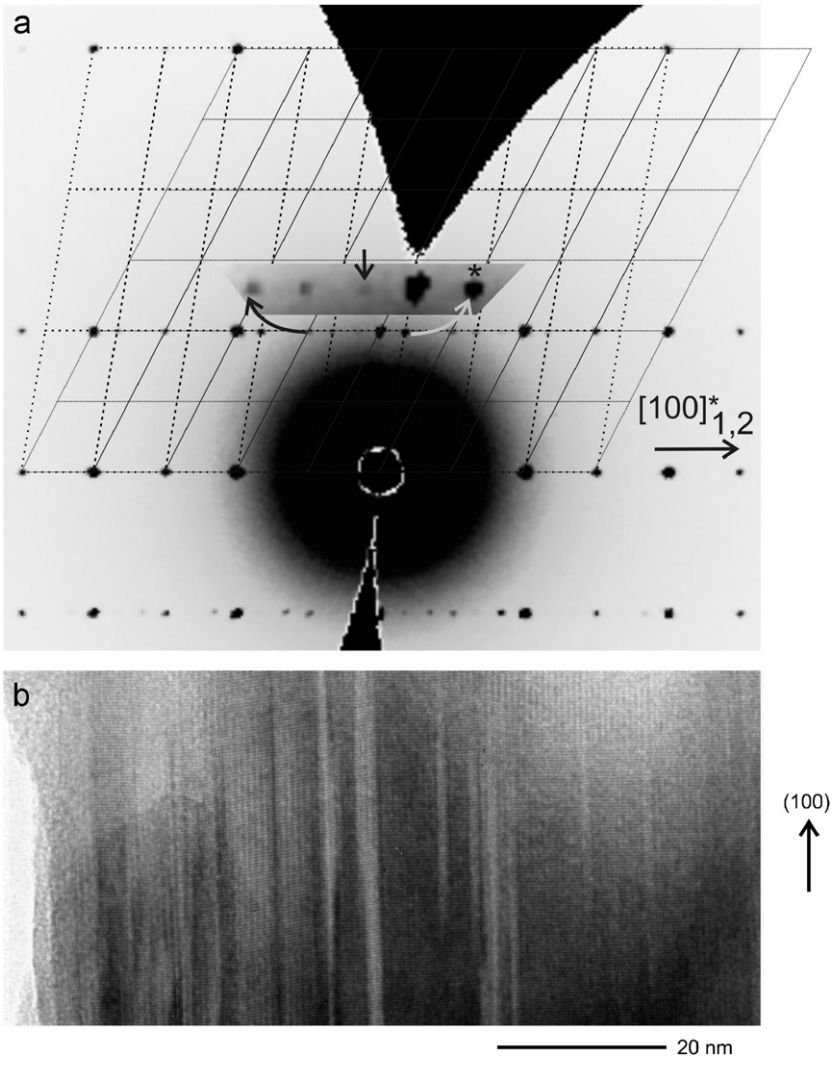

Fig. 1. (a) Section of an X-ray diffraction pattern recorded on a twinned crystal (superposition of $hk0$ and $h0l$). The grids highlight positions of kinematically allowed reflections for $hk0_1$ (solid lines) and $h0l_2$ (broken lines), (b) Bright-field image of a strongly disordered crystal for zone axis [001]; the arrow marks the edge of the (100) lamellae oriented perpendicular to the projection plane.

$c' = 7.2841(3)$ Å, $\beta' = 90.322(2)^\circ$). These metrics correspond to the supposed cell of the superstructure mentioned above, and the symmetry of the superposition patterns can be assigned to space group $P2/c$.

For a first overview of the structure components serving for the superposition in reciprocal space bright field images along the zone axes [0*vw*] were analyzed. All of them show stripes parallel to the plane (100) (see Fig. 1b for [001]), and tilting around [100]* does not change the general appearance of the bright field contrast. Hence, we concluded that (100) lamellae act as the structure components. As an extension of the X-ray experiments nanosized lamellae thinner than the X-ray coherence length were frequently observed.

2.2. HRTEM on Nd_2B_5, characterization of the twin interface

Crystals with broad stripes in the bright field images of [0*vw*] allow analyzing the lamellar crystals sequentially.

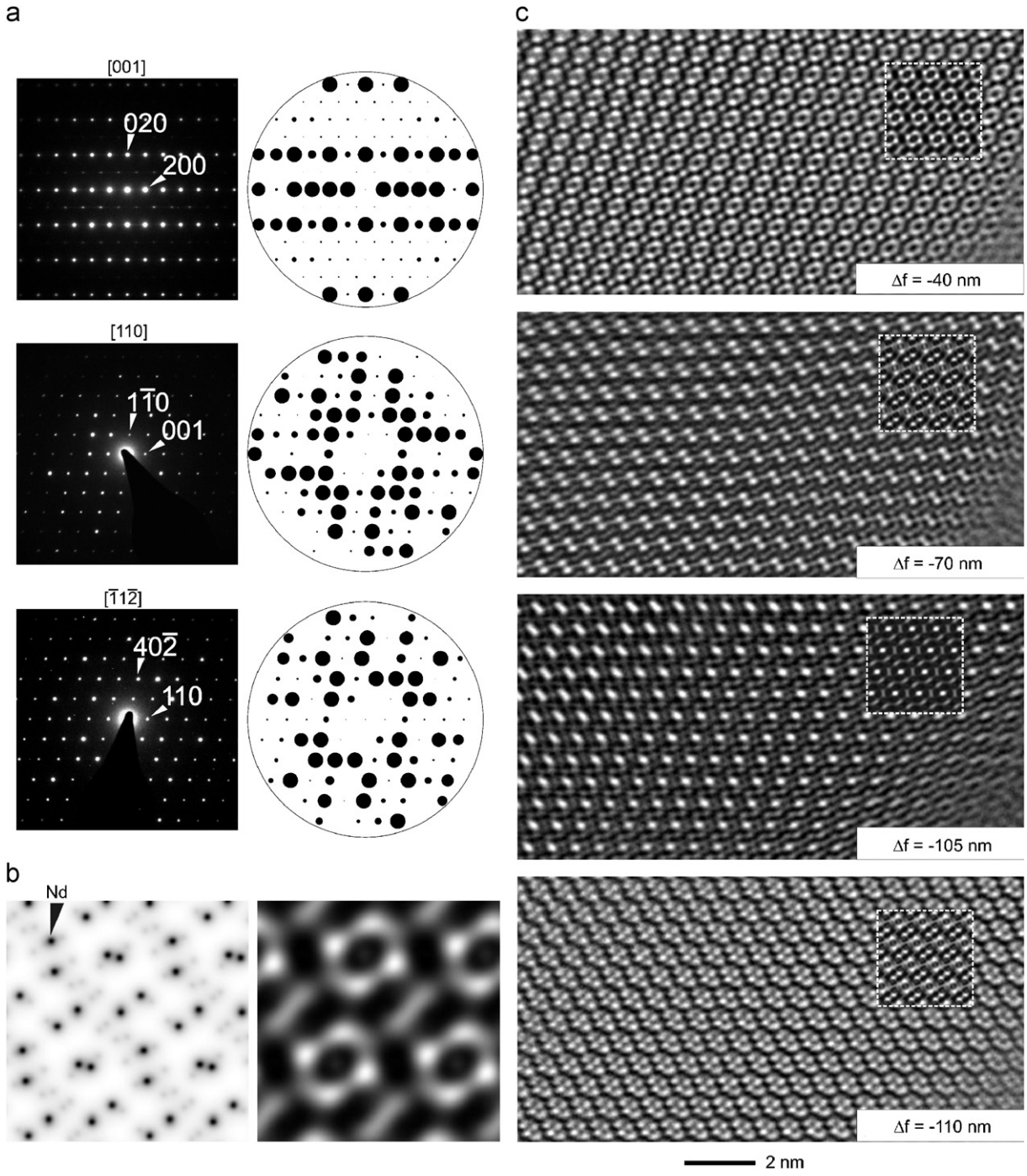

Fig. 2. (a) Experimental and calculated SAED patterns (kinematical approximation) for Nd_2B_5, (b) Comparison of projected potential and simulated micrograph ([112], $t = 7.1$ nm, $\Delta f = -40$ nm), (c) Series of images with variable defocus (see figure) with inserted simulations for [112].

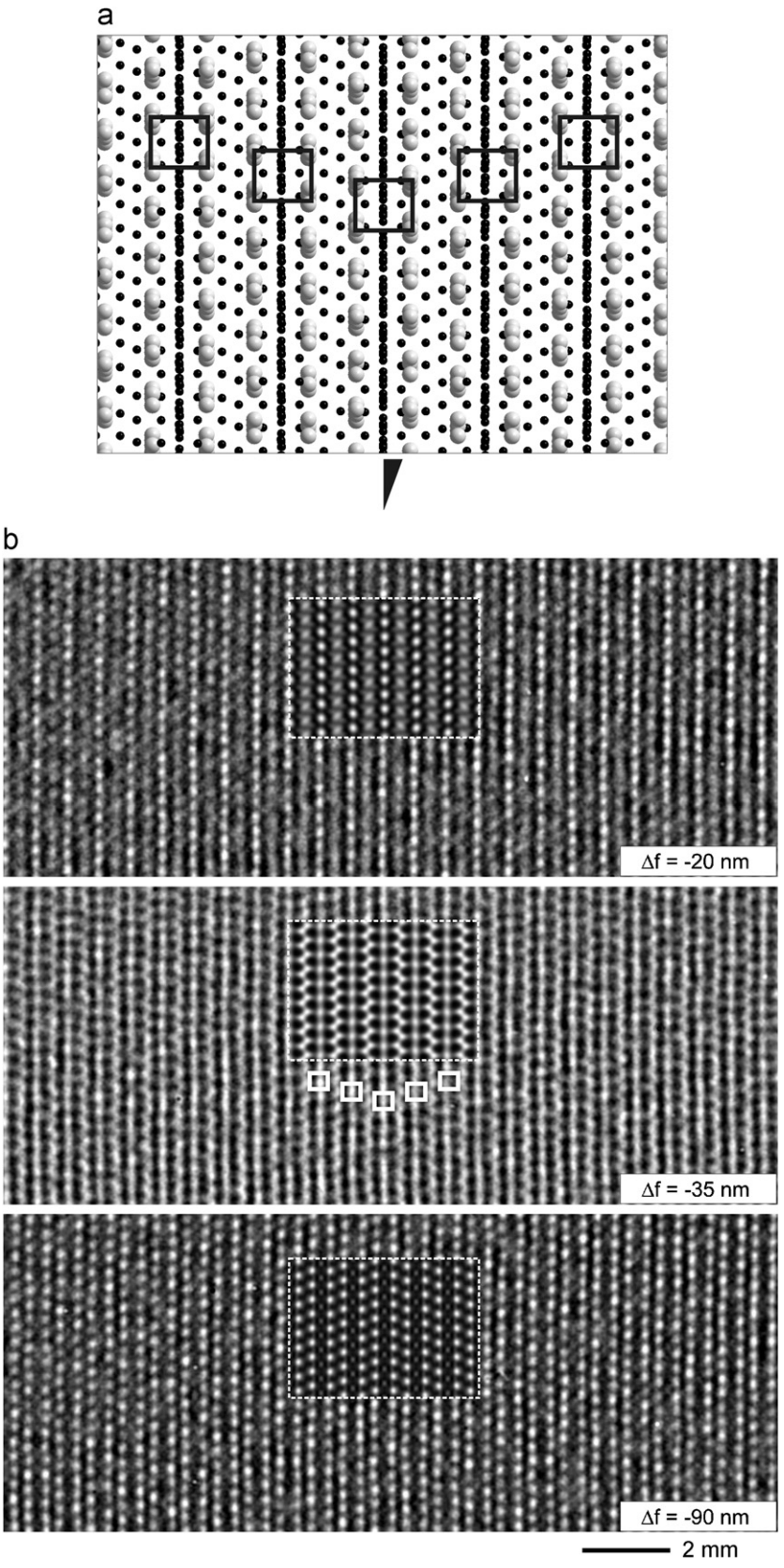

Fig. 3. Twinning in Nd_2B_5 for zone axis [021]. (a) Structure model for the twin interface based on a supercell (scaled to 200% with respect to the experimental images, grey circles: Nd, black circles: B), (b) Series of images with variable defocus (see figure) with inserted simulations ($t = 4.9$ nm).

In addition, tilting perpendicular to [100]* is possible without significant overlap of adjacent lamellae. The SAED patterns of Fig. 2a were recorded on different single lamellae of Nd_2B_5. These diffraction patterns display only the intensities for the Pr_2B_5-type structure and agree well with calculated patterns based on such model. HRTEM gives additional support for the assignment, e.g. for zone axis [112]. The projected potential map (Fig. 2b) is dominated by the strong peaks of the Nd atoms and displays only a marginal discrimination of B atoms and cavities. A close relationship between simulated contrasts and projected potential map is evident, cf. Fig. 2b (left and right), already approximating the imaging conditions of Scherzer focus. The black spots of the simulated micrograph correlate with rows of Nd atoms, white spots with the superposition of cavities and B atoms. In particular for $\Delta f = -40$ nm, the white spots representing the cavities are displayed with a high contrast, cf. the experimental image of Fig. 2c (top) matching the inserted simulated micrograph. Highly negative defocus values inhibit a direct structural interpretation but are of particular importance for detecting minor structural deviations from the model. Those are clearly absent as exemplified by the images of the focus series and the corresponding simulations in Fig. 2c.

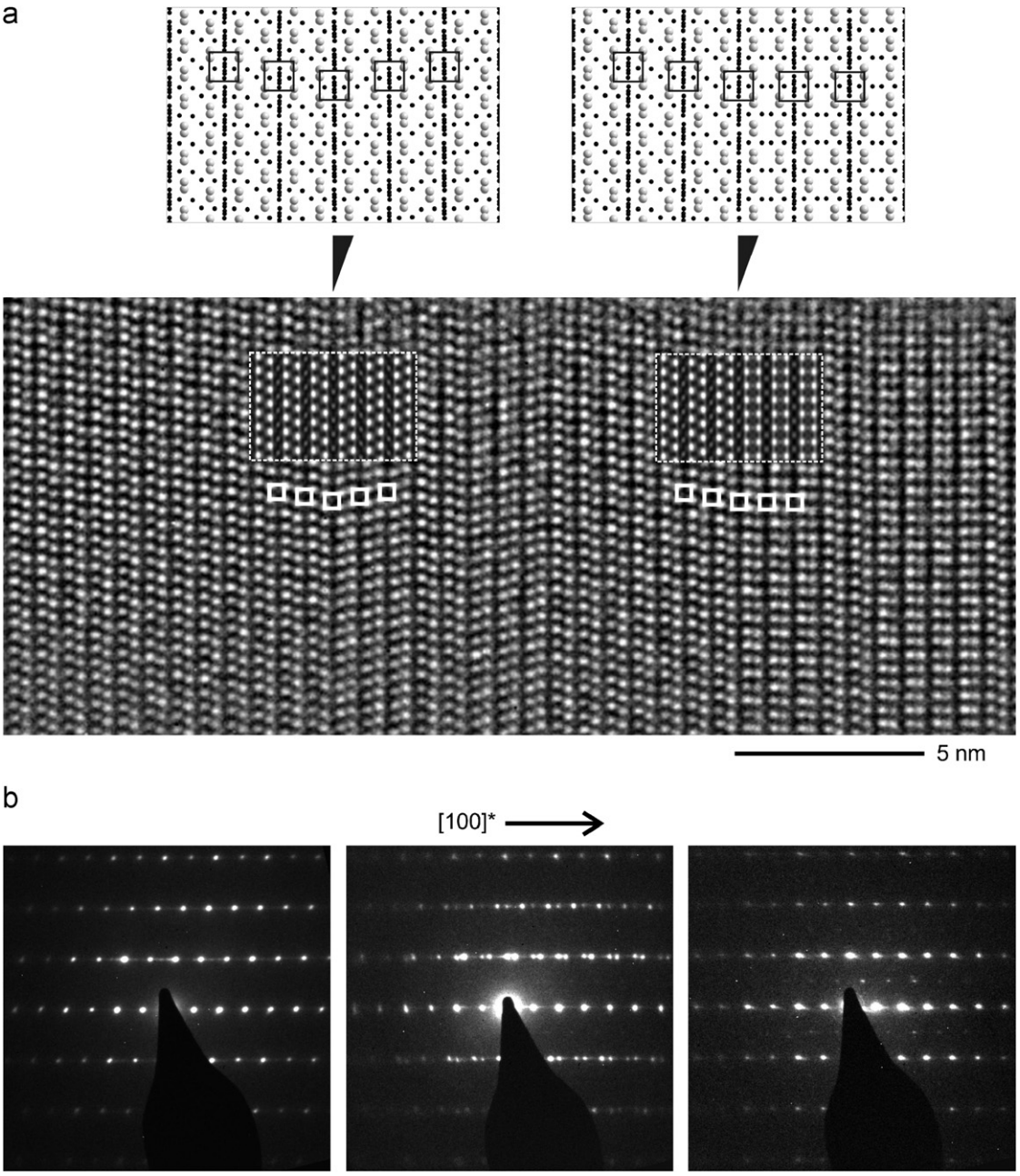

Fig. 4. HRTEM of a twinned area along ⟨010⟩/[001]. (a) Experimental micrograph with inserted simulations ($\Delta f = -90$ nm, $t = 4.4$ nm) and structure projections (scaled to 200% with respect to the experimental images, grey circles: Nd, black circles: B). (b) sequentially recorded SAED patterns of the same crystal (left: zone axis [010], center: superposition pattern, right: zone axis [001]).

All issues concerning the nanosized lamellae can only be derived from HRTEM, in particular, the location and structure of the twin interface. In order to simulate HRTEM images of twinned crystals the structure of Nd_2B_5 was first approximated by a rectangular and triclinic *a*3*b*3*c* supercell close to the pseudo-tetragonal metrics mentioned above (lattice parameters: $a'' = 42.753$ Å, $b'' = c'' = 21.8000$ Å, $\alpha'' = \beta'' = \gamma'' = 90°$). The space group *P*1 was selected to inhibit any symmetry restrictions and to facilitate the incorporation of structure models into the supercell. In the next step structures in the two orientations of the adjacent lamellae were combined to one superposition structure (SPS). Calculated diffraction patterns based on the SPS agree well with experimental patterns if the transmitted areas contain equal ratios of two large lamellae. However, the presence of nanosized lamellae produces deviations, particularly broad diffuse streaks close to the Bragg intensities of the SPS. The diffuse intensities could indicate a marginal strain at the twin interface, vide infra. The positions of the maxima change when distinct areas of the same crystal are analyzed as they depend on the thickness of the lamellae within the transmitted areas. In the final step of the simulation, the two components were separated at the experimentally observed position of the twin interface.

The analyses were facilitated by the large number of crystallites offering zone axes orientations [0*vw*]. The thick lamellae of Fig. 3 (zone axes orientations [021] and [0−2−1]) are rotated by 180° around [100]*. For $\Delta f = -35$ nm (Fig. 3b, center), the dark spots of the HRTEM micrograph correspond to aggregates of Nd atoms. The twinning can be identified by the characteristic arrangement of the black spots, see the squares in Fig. 3a and b (center), respectively. The convincing agreement of the experimental and the inserted simulated micrographs fully supports the proposed structure model. As shown

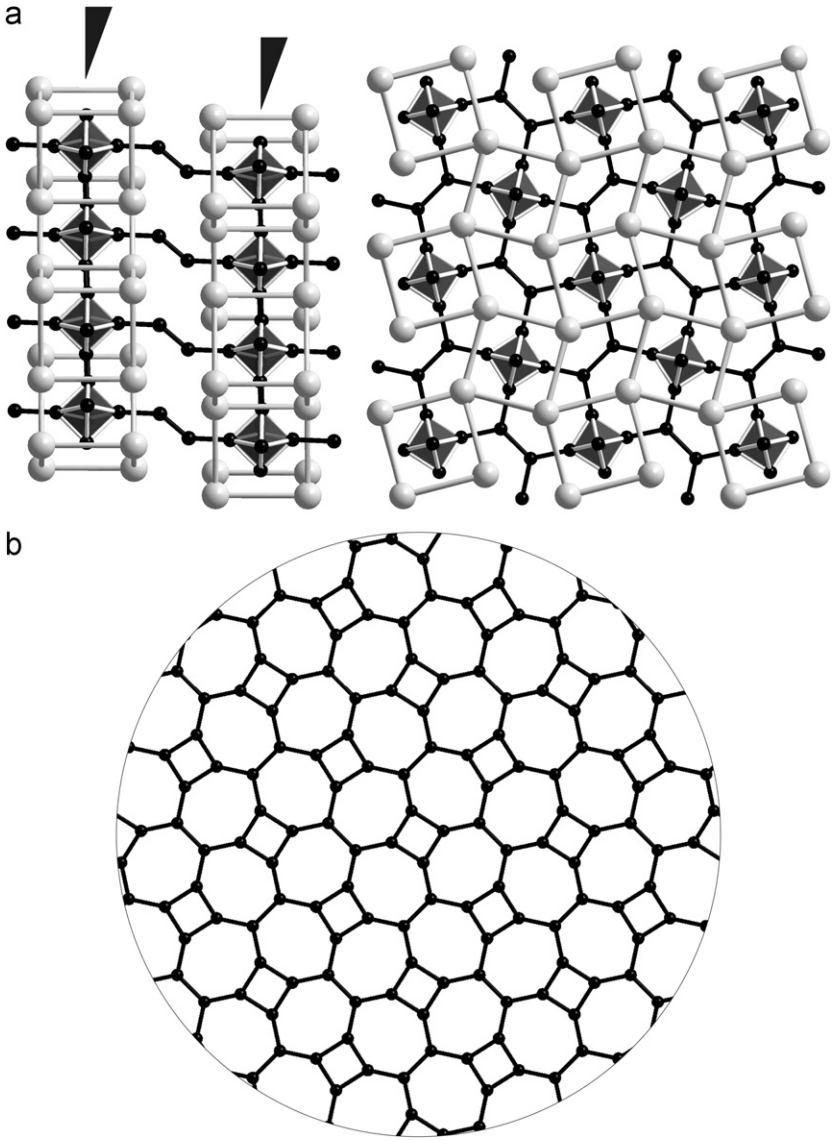

Fig. 5. (a) Left: polyhedral representation of (100) layers in Nd_2B_5, right top view of a single layer (black spheres: B atoms, grey spheres: Nd atoms), (b) Projection of the twin interface on (100).

by simulations, the occurrence of domains in the two other orientations, namely [01−2] and [0−12] (rotation of (100) layers by 90°), could be identified by HRTEM but was not found within this crystallite.

All distinguishable orientations of adjacent lamellae (90° and 180° rotations) are presented in the HRTEM micrograph of Fig. 4 which was recorded along [010] of a main component. Under the selected focus conditions, each

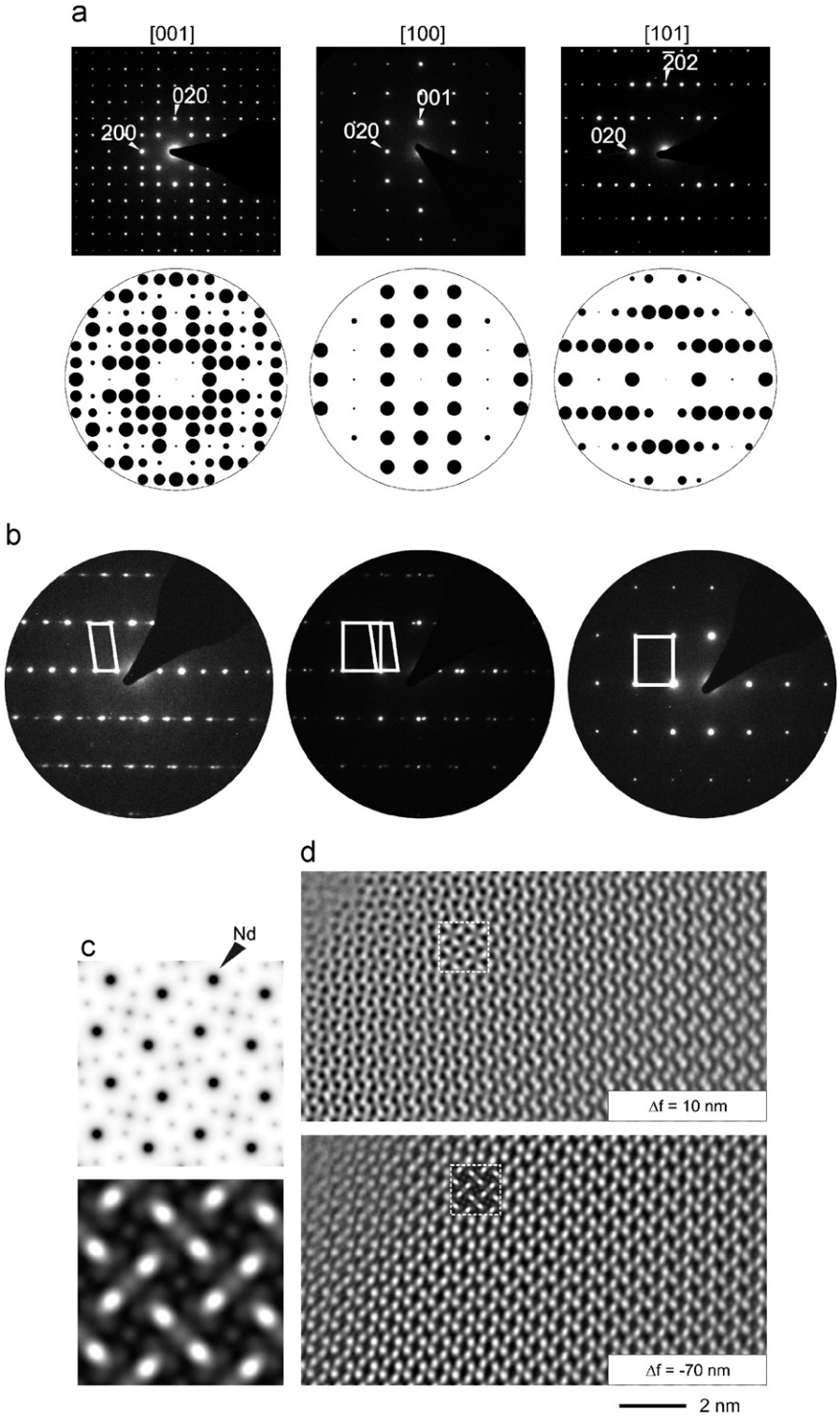

Fig. 6. (a) Experimental and calculated SAED patterns (kinematical approximation) for NdB_4, zone axes specified in the figure, (b) SAED patterns recorded on one lamellar crystal (left: [021] of Nd_2B_5, center: superposition pattern, right: [210] NdB_4), (c) comparison of projected potential map (left) and simulated micrograph for [001] (right, $t = 4.1$ nm, $\Delta f = -70$ nm), (d) images with variable defocus (see figure) for [001] and inserted simulations ($t = 4.1$ nm).

white spot corresponds to two neighboring rows of Nd atoms. On the left, the 180° rotation is shown by the intergrowth of [010]- and [0−10]-lamellae, while on the right [010]- and [001]-orientations of adjacent lamellae are consistent with the rotation of 90°. The SAED patterns of Fig. 4b were recorded on the same crystal but in larger areas mainly containing [010]- (left) and [001]- (right) lamellae, respectively. Fig. 4b (center) shows the superposition pattern which contains the intensities of the separated components and prominent diffuse streaks along [100]*.

The structure at the twin interface can be described with cutouts of polyhedral representations in Fig. 5a. Twin interfaces are restricted to the center of the consecutive (100) layers exemplified in Fig. 5a (left). One of the layers with a composition of NdB_4 (Fig. 5a, right) is composed of slightly distorted cubes of Nd atoms centered by B_6 octahedra and B_2 units serving as interconnection of the B_6 octahedra. As the twin interface cuts the layer in the center, it contains B atoms only, see top view in Fig. 5b. The net of B atoms is sandwiched by two separated square nets of B and Nd atoms, respectively, all of them showing pseudo-fourfold symmetry. Hence, the rotations of the (100) layers at the twin interfaces produce only minor changes of the local partial structures of Nd and B atoms with respect to the untwinned structure. Therefore, only marginal strain is produced by the twinning, and the large number of twin boundaries as well as the occurrence of nanosized lamellae can be understood.

2.3. Characterization of inhomogeneities

Occasionally, we observed single crystallites of a byproduct. The EDX spectra indicate no impurities, therefore we checked for the presence of NdB_4 which was actually identified by SAED, cf. Fig. 6a. Besides single crystallites, the sequential analysis of lamellar crystals point to the coexistence of Nd_2B_5- and NdB_4-lamellae. The

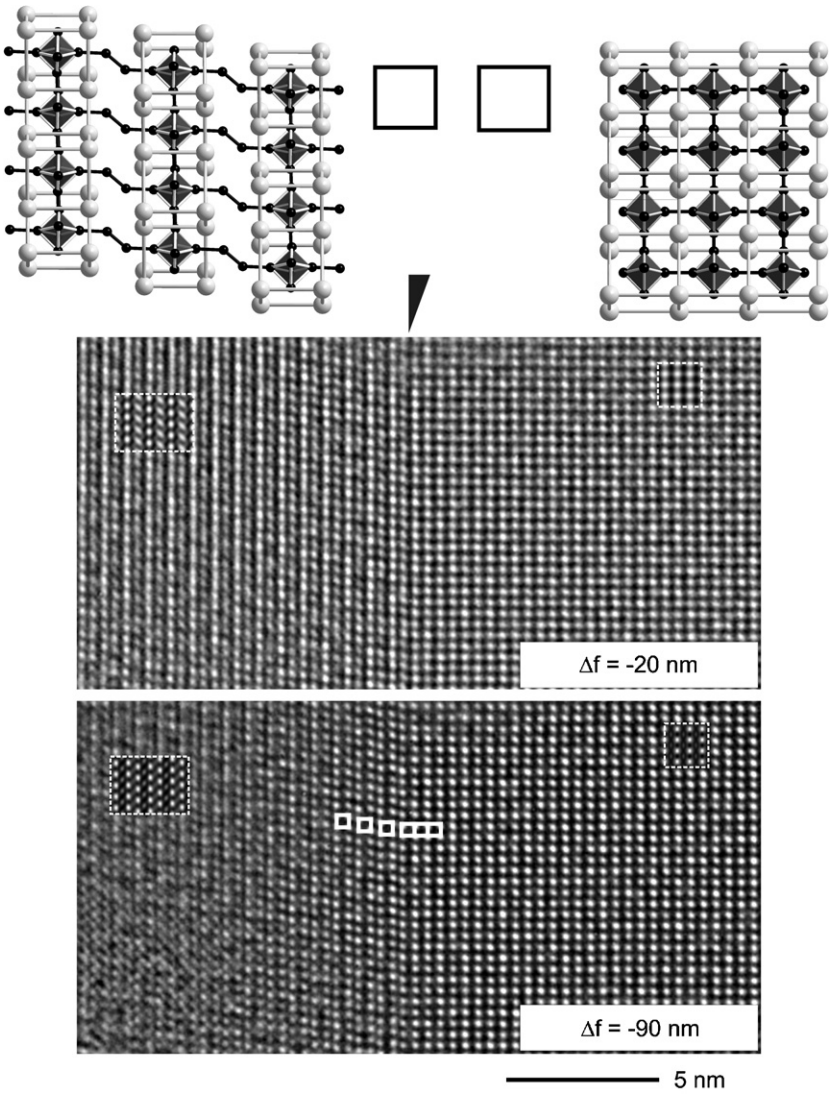

Fig. 7. Chemical intergrowth of Nd_2B_5- and NdB_4-lamellae. Top: polyhedral representations of the components, bottom: HRTEM micrographs with variable defocus (see figure) with inserted simulations (left: Nd_2B_5, [010], right: NdB_4, [100]; $t = 2.2$ nm.

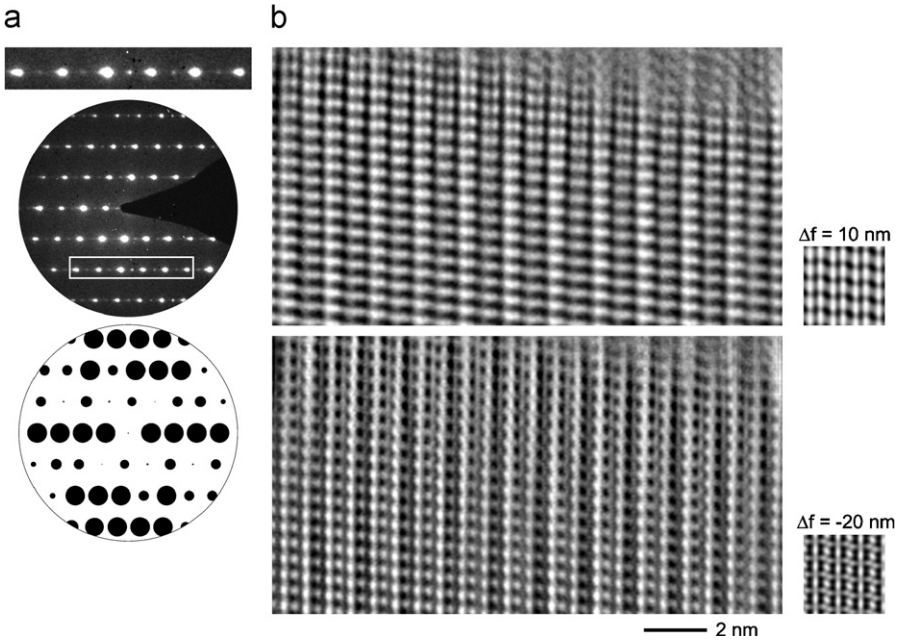

Fig. 8. A new neodymium boride. (a) SAED pattern and calculated pattern of [011] (Nd_2B_5) with enlarged section, (b) HRTEM micrographs for two distinct focus values with attached simulated micrographs based on monoclinic Nd_2B_5 ([011], $t = 3.1$ nm).

superposition pattern in Fig. 6b (center) contains the patterns of twinned Nd_2B_5 [021] and [210] NdB_4, see Fig. 6b left and right, respectively. In contrast to the superposition by twinning, the patterns based on chemical intergrowth show no merohedry, cf. the splitting of the components along [100]* in Fig. 6b (center). Therefore, the chemical intergrowth can easily be identified, even for nanosized lamellae, by the prominent diffuse streaks next to $h\,0\,0(Nd_2B_5)$. Fig. 6c shows the relationship between projected potential map and a simulated micrograph along [001] of NdB_4. For $\Delta f = -70$ nm, the white spots of the simulated micrograph correspond to rows of Nd atoms forming squares. The experimental image of Fig. 6c (top) clearly reproduces the square pattern and matches the inserted simulations, even for variable focus conditions.

The presence of chemically distinct components can also be demonstrated in the case of intergrowth (see the good agreement of experimental and simulated micrographs with the orientations [010] (Nd_2B_5, left) and [100] (NdB_4, right) in Fig. 7). For $\Delta f = -90$ nm, neighboring rows of Nd atoms are imaged as bright spots forming quadrangles. Their dimensions (cf. quadrangles next to the polyhedral representations, Fig. 7, top) and arrangements are characteristically distinct for both structures. Both features are evident from the HRTEM micrographs of Fig. 7. The quadrangles observed for Nd_2B_5 approximate separated squares ($\sim 3.79\,\text{Å} \times 3.79\,\text{Å}$) which are staggered along [100]* while those of NdB_4 are condensed and elongated ($\sim 3.79\,\text{Å} \times 4.10\,\text{Å}$). Both structures contain highly compatible building units, namely the square layers of Nd and B atoms as depicted in the top view of Fig. 5b, left. Such common structural features serve for the fully coherent chemical intergrowth.

Occasionally, an unknown Nd–B component was observed which seems related to Nd_2B_5 by the fundamental reflections of the SAED patterns. However, superstructure reflections along [100]* are present which force a doubling of lattice vector a (Nd_2B_5), see Fig. 8a. To exclude the production of the superstructure reflections by a SPS, tilting experiments and HRTEM were performed. Both show that the superstructure is not an artifact of superposition and underline the relation of the new phase with Nd_2B_5. The simulations based on Nd_2B_5 in Fig. 8b approximate the experimental images; however, they do not show features of the superstructure, e.g. the alternation of bright and dark stripes for $\Delta f = +10$ nm. As demonstrated by Fourier analysis, such details represent the unknown superstructure. Attempts to aggregate the unknown component by variations of nominal composition and reaction conditions are in progress.

3. Conclusions

Crystals of Nd_2B_5 and NdB_4 were described as homogeneous materials on the basis of standard analyses. Our electron microscopy investigations demonstrate that lamellar intergrowth including phasoids are likely to occur. The lamellar structures are based on layered building units which are common for many rare earth metal borides. Therefore, one can also expect related structure phenomena in other fields. The conventional TEM methods applied in this study are not sensitive for identification of variations restricted to the boron substructure; however, such variations seem probable. Therefore, future research should include state-of-the-art electron microscopy techniques,

like the exit wave reconstruction [13], which allow imaging the boron atom.

4. Experimental section

4.1. Synthesis and basic characterization of bulk samples

Polycrystalline samples with the nominal composition Nd_2B_5 were prepared from pure elements: neodymium metal (ingots, >99.9%) and boron (powder, >99%), all supplied by Strem Chemicals. Stoichiometric amounts of the educts were mixed and pressed into pellets. Arc melting of the sample (total: 1 g) was performed on a water-cooled copper hearth under a purified argon atmosphere with Ti/Zr alloy as a getter. To ensure homogeneity of the bulk, the samples were turned over and re-melted several times. Afterwards, the samples were introduced in arc-welded sealed tantalum crucibles under argon (0.5 atm) and heated up to 1770 K for 15 days with the help of a high-frequency furnace (TIG-10/300, Hüttinger, FRG). Finally, they were slowly cooled to room temperature. Single crystals of Nd_2B_5 showed metallic luster and were inert to moisture and air.

Electron microprobe analyses by energy dispersive X-ray spectroscopy (EDX) were conducted with a scanning electron microscope (Jeol JSM-6400) according to the procedure previously reported [14]. The analyses confirmed the presence of only neodymium and boron in the sample.

A small part of the sample was analyzed by X-ray diffraction (XRD) using a powder diffractometer (CPS 120 INEL) equipped with a position-sensitive detector ranging from 6° to 120° in 2θ. The diffraction pattern indicates the presence of Nd_2B_5 as the main component and small impurities of NdB_4.

4.2. Single-crystal X-ray investigations

Single-crystal X-ray data were collected on a STOE IPDS diffractometer (Mo-$K\alpha$ radiation, $C2/c$, $a = 15.0808(7)$, $b = 7.2522(3)$, $c = 7.2841(3)$, $\beta = 109.104(2)$). The program package X-Area 1.18 (Stoe, Darmstadt, 2002) was used for data evaluation.

4.3. Electron microscopy and chemical analysis

HRTEM and SAED were performed with a Philips CM30ST microscope (300 kV, LaB_6 cathode, $C_S = 1.15$ mm). The samples were ground and suspended in n-butanol. One drop of the suspension was placed on a perforated carbon/copper net which served as support for the crystallites. Simulations of HRTEM images (multislice formalism) and of SAED patterns (kinematical approximation) were calculated with the EMS program package [15] (spread of defocus: 70 Å, illumination semiangle: 1.2 mrad). All images were recorded with a Gatan Multiscan CCD camera and evaluated (including Fourier filtering) with the program Digital Micrograph 3.6.1 (Gatan). Elemental analyses by EDX were performed in the nanoprobe and in the scanning mode of CM30ST with a Si/Li detector (Noran, Vantage System).

References

[1] A. Magnéli, Microsc. Microanal. Microstruct. 1 (1990) 1.
[2] L. Kienle, O. Oeckler, Hj. Mattausch, V. Duppel, A. Simon, C. Reiner, M. Schlosser, K. Xhaxhiu, H.J. Deiseroth, Mater. Sci. Semicon. Proc. 6 (2003) 393.
[3] Z.W. Chen, J.K.L. Lai, C.H. Shek, J. Solid State Chem. 178 (2005) 892.
[4] O. Oeckler, J. Bauer, V. Duppel, Hj. Mattausch, A. Simon, Acta Crystallogr. B 58 (2002) 161.
[5] K.E. Spear, Mater. Sci. Technol. 4 (1976) 91.
[6] P.K. Liao, K.E. Spear, M.E. Schlesinger, J. Phase Equilibria 17 (1996) 335.
[7] P. Salamakha, A.P. Gonçalves, O. Sologub, M. Almeida, J. Alloys Compds. 316 (2001) L4.
[8] A. Zalkin, D.H. Templeton, Acta Crystallogr. 6 (1953) 269.
[9] J. Roger, V. Babizetskyy, R. Jardin, J.F. Halet, R. Guérin, J. Alloys Compds. 415 (2006) 73.
[10] C. Schwarz, A. Simon, Z. Naturforsch. 42b (1987) 935.
[11] G.V. Zavalii, Yu.B. Kuz'ma, S.I. Mikhalenko, Poroshk. Metall. 6 (1990) 61.
[12] Yu.B. Kuz'ma, V. Babizhetskyy, R. Guérin, S.I. Mikhalenko, Kristallografiya 48 (2003) 619.
[13] H.W. Zandbergen, D. Tang, J. Jansen, R.J. Cava, Ultramicroscopy 64 (1996) 231.
[14] V. Babizhetskyy, J. Roger, S. Députier, R. Jardin, J. Bauer, R. Guérin, J. Solid State Chem. 177 (2004) 415.
[15] P.A. Stadelmann, Ultramicroscopy 21 (1987) 131.